Carbon concentration, Curie temperature, and magnetic resonance field of Mn5Ge3(C) thin films

E. Assaf, A. Portavoce, M. Descoins, M. Bertoglio, S. Bertaina

Version of Record: https://www.sciencedirect.com/science/article/pii/S2589152919302832
Manuscript_c0a08c7d837e9291472ab2481741a0ff

Carbon concentration, Curie temperature, and magnetic resonance field of $Mn_5Ge_3(C)$ thin films

E. Assaf, A. Portavoce*, M. Descoins, M. Bertoglio, and S. Bertaina

IM2NP, CNRS/Aix-Marseille University, Faculté des Sciences de Saint-Jérôme case 142, 13397 Marseille, France

ABSTRACT

Carbon-doped Mn_5Ge_3 thin films were grown using magnetron sputtering and reactive diffusion or non-diffusive reaction (NDR). The C content, the Curie temperature, and the resonance field difference between the hard and easy axis were measured for all the films, allowing linear relations between these three parameters to be quantitatively determined. Thanks to these functions, the measurement of a single of these parameters allows the two others to be known. The association of the sputtering technique to the NDR process appears as the best way for producing C-doped Mn_5Ge_3 thin films.

Keywords: Mn_5Ge_3, Thin film, Ferromagnetism, Carbon, Doping

*Corresponding author: alain.portavoce@im2np.fr

Ge is currently considered as the most suitable semiconductor for the development of room-temperature (RT) spintronic devices, due to a long electron spin lifetime, a large spin diffusion length, and its possibility of important nonequilibrium spin-polarized electron (SPe) accumulation [1]. Furthermore, Ge is already integrated in the current microelectronics complementary metal oxide semiconductor (CMOS) technology, promising the possible integration of spintronics devices in microelectronics integrated circuits. Direct SPe injection into semiconductors from ferromagnetic metallic layers is generally not as effective as wished, since the metal/semiconductor junction and interfacial states can deteriorate SPe transport [2-5]. However, SPe injection is expected to be improved in the case ferromagnetic layers grown in epitaxy on the semiconductor. Mn_5Ge_3 is a metallic-like ferromagnetic compound [6] that can be grown in epitaxy on Ge(111) [6-7] and Ge(001) [8]. Significant SPe injection from Mn_5Ge_3 thin films has been predicted and demonstrated [9-12], probably due to a relatively small conductivity mismatch between Mn_5Ge_3 and Ge [5, 13-14]. Mn_5Ge_3 thin films can be produced by reactive diffusion (RD) or non-diffusive reaction (NDR) using conventional CMOS processes [12,15-16]. The Mn_5Ge_3 Curie temperature (T_C) lies close to RT [15,17-18], but it can be increased up to temperatures higher than 400 K thanks to C doping [18-23], opening the possibility of RT SPe injection in Ge. Consequently, the influence of C-doping on Mn_5Ge_3 magnetic properties has been extensively studied these past few years. C is expected to occupy octahedral interstitial sites in the Mn_5Ge_3 lattice and to promote a 90° ferromagnetic Mn-C-Mn super-exchange, leading to an increase of T_C [20]. It was experimentally shown that T_C increases linearly with C concentration up to a critical concentration [19,21]. However, the direct comparison between C concentration (C_C) and T_C measured in the same Mn_5Ge_3(C) layer has not been performed to date. Usually, C incorporation in Mn_5Ge_3(C) is assumed to be complete whatever the fabrication methods, and the C concentration contained in the $Mn_5Ge_3C_x$ layer actually refers to the C deposition flux

calibration [18-23]. Thus, large variations were reported concerning the maximum T_C^* and its corresponding critical C concentration x^*: T_C^* ~ 445 K for x^* = 0.5 from Gajdzik et al. [19], while T_C^* ~ 460 K for $0.6 \leq x^* \leq 0.7$ from Spiesser et al. [21], and T_C^* ~ 445 K for x^* = 0.8 from Sürgers et al. [24]. For example, epitaxied Mn_5Ge_3(C) layers are typically grown on Ge during the RD of a C-doped Mn film with the Ge substrate, the C-doped Mn film being usually deposited on Ge at RT by molecular beam epitaxy (MBE) thanks to solid-source Mn and C co-evaporation [6-7,21]. It should be noted that MBE is not used in CMOS technology and the Mn_5Ge_3(C) layer obtained after Mn(C)/Ge RD is assumed to contain the entire C amount incorporated in the initial Mn(C) film. Fig. 1 presents T_C variations versus the carbon concentration expected to be incorporated in Mn_5Ge_3(C) films reported in the literature. A recent work showed a significant difference between the T_C of Mn_5Ge_3 layers obtained by RD or NDR using the same sputtering deposition conditions [16]. This work suggests that i) part of the C contained in the initial Mn(C) film is not incorporated in Mn_5Ge_3 during RD, ii) NDR allows a higher level of C incorporation in Mn_5Ge_3, iii) the CMOS-compatible sputtering deposition technique is preferable to the MBE technique as it allows high-T_C Mn_5Ge_3 layers to be grown without the use of C flux, and iv) a relation exists between C_C, T_C, and the magnetic resonance field of the film. The present work aims to determine the reason for the high T_C of sputtering-mediated Mn_5Ge_3 films obtained by NDR, and to quantitatively determine the relation between the C content, the Curie temperature and the magnetic resonance field of Mn_5Ge_3(C) thin films.

Five Mn_5Ge_3 nano-films of same thickness were grown on the native oxide of a Si(001) substrate following two steps: i) RT atomic deposition, and ii) ex situ annealing under vacuum ($P \leq 10^{-7}$ Torr) at T = 673 K. All the samples were made in the same magnetron sputtering system exhibiting a base pressure of 10^{-8} Torr, using a 99.9999% pure Ar gas flow to sputter a 99.99% pure Ge target and a 99.9% pure Mn target. For the first sample (#1), a

30 nm-thick Mn layer was deposited on a 200 nm-thick Ge layer, and the Mn_5Ge_3 nano-film was grown by RD [15-16]. For the rest of the samples (sample #2 to #5), an amorphous $Mn_{0.625}Ge_{0.375}$ film was deposited on the SiO_2 layer thanks to Mn and Ge co-sputtering, and the Mn_5Ge_3 nano-film was grown by NDR during 10 min-long thermal annealing [16]. C was not "actively" deposited on the substrate during Mn and Ge co-deposition (no C flux). However, the sputtering conditions were adjusted for each of these $Mn_{0.625}Ge_{0.375}$ films in order to deposit each time a film exhibiting the same stoichiometry and the same thickness but for different deposition time (t_D), as "passive" impurity incorporation (such as C) is expected to increase with deposition time in sputtered layers. t_D is given for each sample in the second column of Tab. 1. The thickness of the Mn_5Ge_3 layers was measured by X-ray reflectivity and was found to be 47 ± 5 nm. The film structure was checked by X-ray diffraction (XRD) in the Bragg-Brentano geometry using a Cu $K\alpha$ source ($\lambda_{K\alpha}$ = 0.154 nm). The film composition was determined thanks to laser-pulsed atom probe tomography (APT) measurements performed at T = 30 K using a CAMECA LEAP 3000X HR microscope, with a laser pulse frequency of 100 kHz and a laser power of 0.6 nJ. The variations of the film magnetization versus temperature was measured using a superconducting quantum interference device (SQUID) magnetometer Quantum Design MPM-SXL, and the ferromagnetic resonance (FMR) of the samples was studied at RT using a conventional Bruker EMX spectrometer operating at f = 9.39 GHz.

After reaction, the X-ray diffractograms show only diffraction peaks belonging to the Mn_5Ge_3 compound. In the case of sample #2, the diffractogram presented in Fig. 2a displays also some Ge peaks of low intensity. The presence of pure Ge crystallites in this film is attributed to a slight stoichiometry deviation during atomic deposition, probably resulting from the deposition beginning at the Mn and Ge shutter opening, accentuated by the short deposition time t_D = 3.43 min. All the Mn_5Ge_3 films are polycrystalline, XRD measurements

showing several diffraction peaks corresponding to different crystalline orientations. Seven diffraction peaks belonging to the Mn_5Ge_3 film are observed in Fig. 2a at $2\theta = 30.9°$, 35.8°, 38.7°, 42.7°, 43.8°, 46.3°, and 56.7°, corresponding respectively to the atomic planes (111), (002), (210), (211), (112), (202), and (311) of the Mn_5Ge_3 hexagonal structure. Fig. 2b presents a volume of sample #2 analyzed by APT. Each point is a single atom: green, red, and brown for Mn, Ge, and C atoms, respectively. 5 O at% (blue) and 2 Mn at% (green) iso-concentration surfaces are also displayed in the volume, revealing the presence of MnO_y clusters in the layer [25]. Excepted sample #1 grown by RD, all the samples grown by NDR contain MnO_y clusters. These clusters result from periodic Mn and Ge concentration variations in the as-deposited amorphous $Mn_{0.625}Ge_{0.375}$ film, due to the rotation of the sample (5 rpm) during co-sputtering from the two Mn and Ge targets [25]. In order to determine the composition of the Mn-Ge layers, all the atoms belonging to the MnO_y clusters were removed from the APT volumes before to measure the Mn, Ge, and C concentrations, using both atomic concentration average calculated on the entire volume, and concentration profiles measured in the thickness of the films. The concentrations determined by these two methods were found to be in agreement within each sample. For example, Fig. 2c shows a 5 nm-thick slice taken in the APT volume presented in Fig. 2b after removing the clusters from the volume, and Fig. 2d presents the Mn (green solid squares), Ge (red open squares), and C (brown solid stars) concentration profiles measured in the entire volume (Fig. 2b) without clusters. The Mn and Ge concentrations measured in each sample were found to correspond to the Mn_5Ge_3 compound stoichiometry (Fig. 2d) in agreement with XRD measurements (Fig. 2a). C atoms were found to be homogeneously distributed in the $Mn_5Ge_3(C)$ films (Fig. 2d). The C concentration could not be determined in sample #1 due to a concentration lower than the APT detection limit (~ 0.01 at%). The C concentrations measured in the other samples are given in Tab. 1. The magnetization variation of each sample versus temperature

was measured by SQUID between 2 and 430 K, allowing the T_C to be determined for each sample. As expected [15-16], the Mn_5Ge_3 layer grown by RD (sample #1) exhibits a T_C = 297 K corresponding to the standard (undoped) Mn_5Ge_3 compound. Fig. 3a presents the magnetization evolution of sample #2 versus temperature. The Curie temperature of this sample was found to be ~ 317 K. The T_C measured in each sample is reported in Tab. 1. Finally, the angular (θ_H) variation of the magnetic resonance field (Hr) was studied at RT for each sample. Fig. 3b presents Hr variations versus θ_H for sample #2. The measurements confirmed that all the samples possess a shape anisotropy with an easy axis ($Hr_{//}$) in the direction parallel to the surface (θ_H = 90°) and a hard axis ($Hr_{\perp} > Hr_{//}$) in the direction perpendicular to the surface (θ_H = 0°) due to the film geometry. As shown in Fig. 3b, the FMR measurements can be well simulated using the Chappert model [26] (red solid line in Fig. 3b) containing only two magnetic anisotropies: the shape anisotropy and the magneto-crystalline anisotropy. The resonance field difference $\Delta Hr = Hr_{\perp} - Hr_{//}$ between the hard and easy axis was then determined from the FMR measurements for the different samples. Tab. 1 gathers the different value of t_D, C_C, T_C, and ΔHr measured in each of the samples. As expected, the C concentration in the Mn_5Ge_3(C) layers grown by NDR (sample #2 to #5) increases with sputtering deposition time, demonstrating the possibility of controlling C incorporation in the Mn_5Ge_3(C) layers by adjusting the sputtering conditions, without the use of C co-deposition, reducing device contamination risk. The Mn_5Ge_3(C) Curie temperature increases with the C concentration from its standard value T_C = 297 K in sample #1 up to T_C = 420 K in sample #5 exhibiting the longer sputtering deposition time t_D = 20.67 min and the highest C content C_C = 2.35 at%. Tab. 1 shows also that the magnetic resonance field difference between the hard and easy axis measured at 300 K increases with C concentration, following the behavior of T_C. As expected, higher T_C corresponds to higher ΔHr. Fig. 4 presents the plot of T_C and ΔHr versus C_C. T_C and ΔHr are strictly proportional to C_C.

Mn_5Ge_3(C) Curie temperature as well as the magnetic resonance field difference increase linearly with the C concentration, leading also to a linear relation between T_C and ΔHr, as shown in the Fig. 4 inset. Our measurements give the following three functions:

$$T_C = 298.84 + 51.79 \times C_C \quad (1)$$

$$\Delta Hr = 1.69 + 2.27 \times C_C \quad (2)$$

$$\Delta Hr = 0.044 \times T_C - 11.40 \quad (3)$$

with C_C in at%, T_C in K, and ΔHr in kOe. Eq. 1, 2, and 3 allow the set of the three parameters Curie temperature, C concentration, and magnetic resonance field difference between the hard and easy axis at 300 K to be known from the measurement of only a single of these parameters. Our measurements concerning the variation of T_C with C_C (short-dash line) are compared to the literature in Fig. 1. Despite a large disagreement with the main part of the data from the literature, one can note that our measurements are not too different from the data reported by Dutoit et al. (solid triangles) in ref. [23]. In this work, monocrystalline MnCoGe(C) films were grown on Ge(111) using the "reactive deposition epitaxy" (RDE) method, which is actually similar to NDR, using MBE co-deposition of Mn, Ge, and C. In this case, in agreement with our results, the C concentration incorporated in the films is closer to the initial C concentration deposited by evaporation, determined from C flux calibrations and reported by the authors. This interpretation is also in agreement with the data reported by Petit et al. in ref. [7] (open squares in Fig. 1). Indeed, except the measurement performed on undoped Mn_5Ge_3, the only measurement in agreement with our data (red arrow in Fig. 1) corresponds to the growth of Mn_5Ge_3(C) by RDE instead of RD. The small disagreement between our measurements and ref. [23] and [7] should be due to C flux calibration errors and the difference between the initial C content and the final C incorporation in the film after

reaction. T_C = 420 K for C_C ~ 2.35 at% is not too far from T_C^*, and Eq. 1 predicts that the maximum T_C^* = 445–460 K reported in the literature corresponds to a C doping of C_C ~ 2.8–3.1 at% that corresponds to x^* ~ 0.23–0.26. However, in the case of RD, the highest T_C obtained by C doping is regularly reported for $x^* \geq 0.6$, the C concentration being referred to the initial C content in the Mn film deposited on Ge before RD [18,21]. $Mn_5Ge_3C_{0.6}$ corresponds to C_C ~ 7 at%, meaning that more than half of the C contained in the initial Mn layer is not activated in Mn_5Ge_3(C), probably due to the concurrent phenomena of RD purification [27] and Mn carbide cluster formation [21]. The use of RD with high C content in the Mn layer may be detrimental to the desired electrical and magnetic properties, as part of the extra C not incorporated in Mn_5Ge_3(C) is expected to be pushed-off towards the Mn_5Ge_3(C)/Ge interface [27], and can trigger the formation of Mn carbide clusters if the C solubility is locally reached in the Mn_5Ge_3(C) film [21]. It should be noted that these Mn-C clusters are sometimes very difficult to detect even by high resolution transmission electron microscopy due to very small sizes [28]. Consequently, NDR appears as a better method for C incorporation into Mn_5Ge_3. The MnO_y clusters present in the NDR-mediated Mn_5Ge_3(C) films should be avoided without the rotation of the sample during deposition, using a sputtering setup with a different geometry between the targets and the substrate. These clusters have no noticeable effect on the magnetic properties of the Mn_5Ge_3(C) films [29]. However, they may have an effect on SPe injection. Sample #1 (without cluster and C_C ~ 0 at%) and sample #3 (with clusters and C_C = 0.90 at%) were grown on an insulating glass substrate, in order to measure their resistivity (ρ) at RT using a four-point probe. The resistivity of the sample #3 ($\rho = 7.4 \times 10^{-3}$ Ω cm) is three times higher than the resistivity of the sample #1 ($\rho = 2.5 \times 10^{-3}$ Ω cm). However, the contribution of the MnO_y clusters on electron scattering is difficult to determine, since Mn_5Ge_3(C) resistivity was shown to be higher than that of Mn_5Ge_3 [13]. Furthermore, the resistivity of our Mn_5Ge_3(C) film is found about 18 times smaller than the

resistivity reported in ref. [13] in the case of a cluster-free 50 nm-thick $Mn_5Ge_3C_{0.8}$ film grown at $673 \leq T \leq 773$ K by sputtering on a sapphire substrate.

In conclusion, C-doped Mn_5Ge_3 nano-films were grown using RD and NDR. Mn or amorphous $Mn_{0.625}Ge_{0.375}$ layers were deposited on SiO_2 using magnetron sputtering of Ge and Mn targets before to be annealed at 673 K. The sputtering time of the $Mn_{0.625}Ge_{0.375}$ films was varied in order to obtain Mn_5Ge_3(C) layers exhibiting different levels of C doping. Thus, the Mn_5Ge_3(C) films were characterized by XRD, APT, SQUID, and FMR, aiming to determined their C content as well as their Curie temperature and their magnetic resonance fields along their easy and hard axis. These measurements confirmed that the high T_C of sputtering-mediated Mn_5Ge_3 films obtained by NDR is due to C incorporation from the residual vacuum in the sputtering chamber. Furthermore, the possibility of controlling the C doping level in the Mn_5Ge_3(C) films by controlling the sputtering conditions was demonstrated, as C doping levels from 0.27 to 2.35 at% were obtained, corresponding to $317 \leq T_C \leq 420$ K. As expected, RD is shown to prevent the entire C content of the initial Mn(C) layer to be incorporated into the Mn_5Ge_3(C) film obtained after the reaction between Mn(C) and Ge. The C concentration of the layer obtained by RD was shown to be lower than 0.01 at% and to exhibit the conventional $T_C = 297$ K of undoped Mn_5Ge_3. The C concentration C_C, the Curie temperature T_C and the resonance field difference ΔHr between the hard and easy axis are found to be proportional, and the linear functions linking T_C and ΔHr to C_C, as well as ΔHr to T_C were determined.

This work was supported by the French government through the program "Investissements d'Avenir A*MIDEX" [Project APODISE, no. ANR-11-IDEX-0001-02] managed by the National Agency for Research (ANR).

Declaration of interest - None

REFERENCES

[1] F. Bottegoni, C. Zucchetti, S. Dal Conte, J. Frigerio, E. Carpene, C. Vergnaud, M. Jamet, G. Isella, F. Ciccacci, G. Cerullo, and M. Finazzi, Phys. Rev. B 118 (2017) 167402.

[2] M. Tran, H. Jaffrès, C. Deranlot, J.-M. George, A. Fert, A. Miard, and A. Lemaître, Phys. Rev. Lett. 102 (2009) 036601.

[3] O. Txoperena, Y. Song, L. Qing, M. Gobbi, L.E. Hueso, H. Dery, and F. Casanova, Phys. Rev. Lett. 113 (2014) 146601.

[4] S. Sharma, A. Spiesser, S. P. Dash, S. Iba, S. Watanabe, B. J. van Wees, H. Saito, S. Yuasa, and R. Jansen, Phys. Rev. B 89 (2014) 075301.

[5] T. Schäpers, Semiconductor Spintronics, Walter de Gruyter GmbH, Berlin/Boston, 2016.

[6] C. Zeng, S.C. Erwin, L.C. Feldman, A.P. Li, R. Jin, Y. Song, J.R. Thompson, and H.H. Weitering, Appl. Phys. Lett. 83 (2003) 5002.

[7] M. Petit, L. Michez, C.-E. Dutoit, S. Bertaina, V.O. Dolocan, V. Heresanu, M. Stoffel, V. Le Thanh, Thin Solid Films 589 (2015) 427.

[8] Y. Xie, Y. Yuan, M. Wang, C. Xu, R. Hübner, J. Grenzer, Y.-J. Zeng, M. Helm, S. Zhou, and S. Prucnal, Appl. Phys. Lett. 113 (2018) 222401.

[9] S. Picozzi, A. Continenza, and A.J. Freeman, Phys. Rev. B 70 (2004) 235205.

[10] R.P. Panguluri, C. Zeng, H.H. Weitering, J.M. Sullivan, S.C. Erwin, and B. Nadgorny, Phys. Stat. Sol. (b) 242 (2005) R67.

[11] Yu.S. Dedkov, M. Holder, G. Mayer, M. Fonin, and A.B. Preobrajenski, J. Appl. Phys. 105 (2009) 073909.

[12] I.A. Fischer, L.-T. Chang, C. Sürgers, E. Rolseth, S. Reiter, S. Stefanov, S. Chiussi, J. Tang, K.L. Wang, and J. Schulze, Appl. Phys. Lett. 105 (2014) 222408.

[13] I.A. Fischer, J. Gebauer, E. Rolseth, P. Winkel, L.-T. Chang, K.L. Wang, C. Sürgers, and J. Schulze, Semicond. Sci. Technol. 28 (2013) 125002.

[14] E.I. Rashba, Phys. Rev. B 62 (2000) R16 267.

[15] O. Abbes, A. Portavoce, V. Le Thanh, C. Girardeaux, and L. Michez, Appl. Phys. Lett. 103 (2013) 172405.

[16] E. Assaf, A. Portavoce, K. Hoummada, M. Bertoglio, and S. Bertaina, Appl. Phys. Lett. 110 (2017) 072408.

[17] E. Sawatzky, J. Appl. Phys. 42 (1971) 1706.

[18] A. Spiesser, V. Le Thanh, S. Bertaina, and L.A. Michez, Appl. Phys. Lett., Vol. 99 (2011) 121904.

[19] M. Gajdzik, C. Sürgers, M.T. Kelemen, and H.v. Löhneysen, J. Magnetism and Magnetic Materials 221 (2000) 248.

[20] I. Slipukhina, E. Arras, Ph. Mavropoulos, and P. Pochet, Appl. Phys. Lett. 94 (2009) 192505.

[21] A. Spiesser, I. Slipukhina, M.-T. Dau, E. Arras, V. Le Thanh, L. Michez, P. Pochet, H. Saito, S. Yuasa, M. Jamet, and J. Derrien, Phys. Rev. B 84 (2011) 165203.

[22] L.-A. Michez, F. Virot, M. Petit, R. Hayn, L. Notin, O. Fruchart, V. Heresanu, M. Jamet, and V. Le Thanh, J. Appl. Phys. 118 (2015) 043906.

[23] C.-E. Dutoit, V.O. Dolocan, M. Kuzmin, L. Michez, M. Petit, V. Le Thanh, B. Pigeau, and S. Bertaina, J. Phys. D: Appl. Phys. 49 (2016) 045001.

[24] C. Sürgers, K. Potzger, T. Strache, W. Möller, G. Fischer, N. Joshi, and H. v. Löhneysen, Appl. Phys. Lett. 93 (2008) 062503.

[25] A. Portavocea, E. Assaf, C. Alvarez, M. Bertoglio, R. Clérac, K. Hoummada, C. Alfonso, A. Charaï, O. Pilone, K. Hahn, V. Dolocan, and S. Bertaina, Appl. Surf. Sci. 437 (2018) 336.

[26] C. Chappert, K. Le Dang, P. Beauvillain, H. Hurdequint, and D. Renard, Phys. Rev. B 34 (1986) 3192.

[27] K. Hoummada, I. Blum, D. Mangelinck, A. Portavoce, Appl. Phys. Lett. 96 (2010) 261904.

[28] A. Portavoce, O. Abbes, A. Spiesser, C. Girardeaux, L. Michez, and V. Le Thanh, Scripta Mater. 100 (2015) 70.

[29] E. Assaf, Ph. D. Thesis, Aix-Marseille University, 2019.

Figure 1

E. Assaf et al.

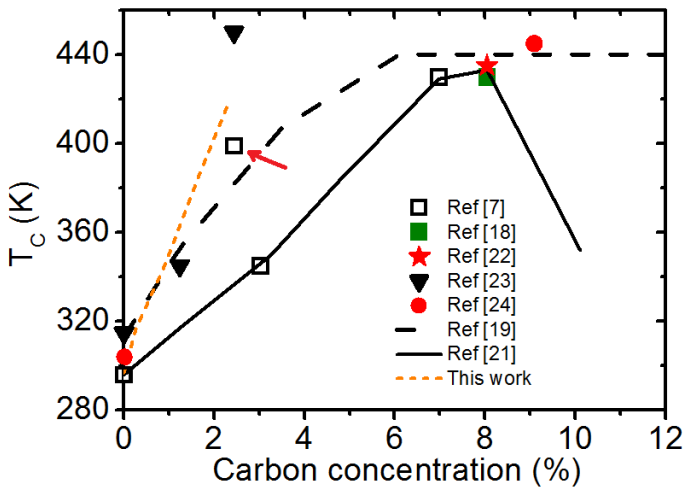

FIG. 1. Variations of the Curie temperature (T_C) of $Mn_5Ge_3(C)$ thin films versus carbon concentration reported in the literature. Our measurements are also plotted for comparison (short dash line). The carbon concentration was measured in each film in our case, while it corresponds to the carbon flux calibration used for deposition in the cases reported in the literature.

Figure 2

E. Assaf et al.

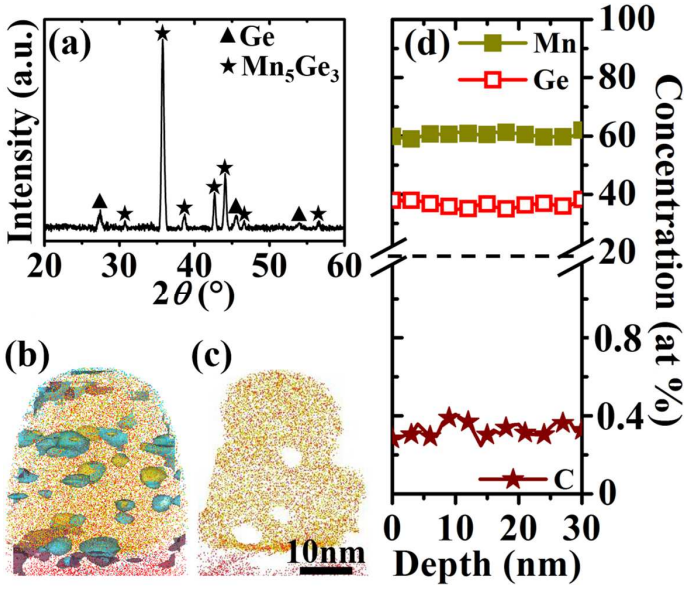

FIG. 2. Structural and chemical analyses performed on sample #2 after reaction: a) XRD measurements performed at RT; b) sample volume analyzed by APT, green, red, and brown dots correspond respectively to Mn, Ge, and C atoms, the blue and green surfaces correspond respectively to 5 O at% and 2 Mn at% iso-concentration surfaces, c) 5 nm-thick slice taken in the same APT volume after removing the atoms comprised in the O and Mn iso-concentration surfaces; and d) Mn (solid squares), Ge (open squares), and C (solid stars) concentration profiles measured in the same volume after removing the atoms comprised in the O and Mn iso-concentration surfaces.

Figure 3

E. Assaf et al.

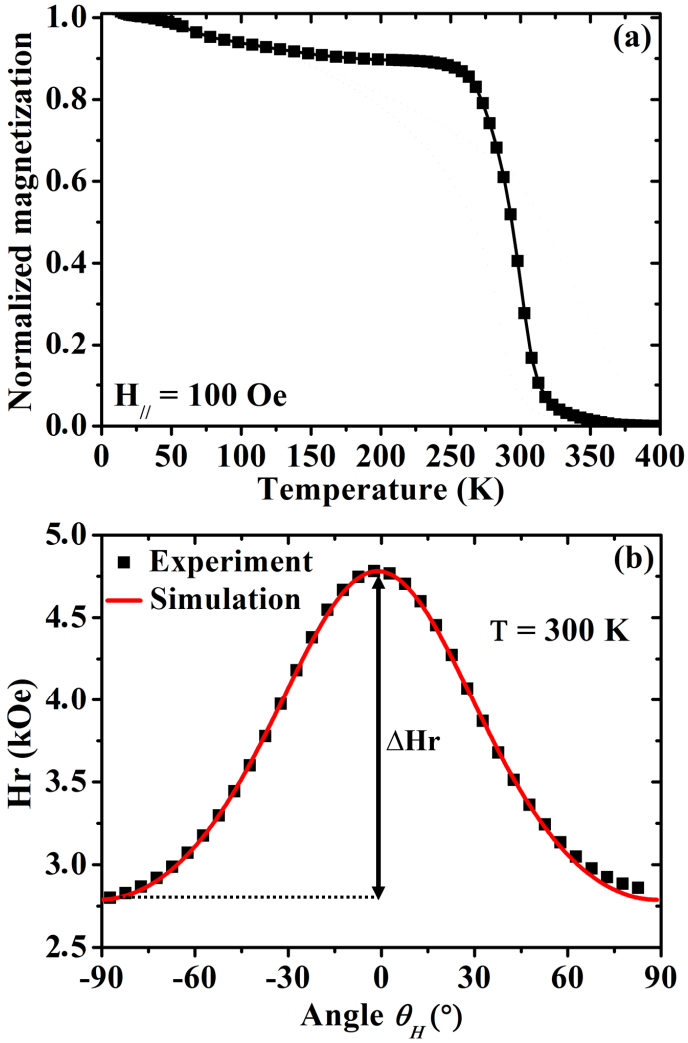

FIG. 3. Magnetic properties of sample #2: a) Magnetization evolution versus temperature with a magnetic field ($H_{//}$) of 100 Oe applied in-plane (T_C ~ 317 K), and b) angular variation (θ_H) of the resonance field (Hr) measured by FMR. The red solid line corresponds to a simulation using the Chappert model [26].

Figure 4

E. Assaf et al.

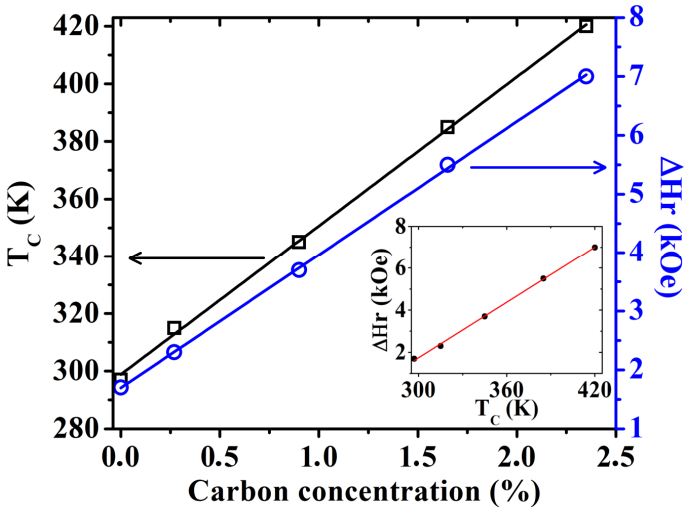

FIG. 4. Variations of T_C and ΔHr of a polycrystalline Mn_5Ge_3 nano-films versus their C doping concentration. The inset presents the corresponding variation of ΔHr versus T_C measured in the Mn_5Ge_3 nano-films containing different C concentrations.

Table 1

E. Assaf et al.

Sample	t_D (min)	C_C (at%)	T_C (K)	ΔHr (kOe)
#1	–	< 0.01	297	1.7
#2	3.43	0.27	317	2.3
#3	10.33	0.90	345	3.7
#4	15.73	1.65	385	5.5
#5	20.67	2.35	420	7.0

TAB. 1. Summary of the different parameters (deposition time–t_D, carbon concentration–C_C, Curie temperature–T_C, and hard and easy axis resonance field difference–ΔHr) measured in five different Mn_5Ge_3 nano-layers (sample #1 to #5) elaborated using magnetron sputtering deposition followed by ex situ annealing at 673 K under vacuum.